

Competition between photochemistry and energy transfer in ultraviolet-excited diazabenzenes. I. Photofragmentation studies of pyrazine at 248 nm and 266 nm

Eric T. Sevy, Mark A. Muyskens, Seth M. Rubin, George W. Flynn, and James T. Muckerman

Citation: *The Journal of Chemical Physics* **112**, 5829 (2000); doi: 10.1063/1.481157

View online: <http://dx.doi.org/10.1063/1.481157>

View Table of Contents: <http://scitation.aip.org/content/aip/journal/jcp/112/13?ver=pdfcov>

Published by the [AIP Publishing](#)

Articles you may be interested in

Communication: Trapping upconverted energy in neat platinum porphyrin films via an unexpected fusion mechanism

J. Chem. Phys. **139**, 101102 (2013); 10.1063/1.4821164

H atom formation from benzene and toluene photoexcitation at 248 nm

J. Chem. Phys. **131**, 204304 (2009); 10.1063/1.3262701

Intermolecular energy transfer involving an iridium complex studied by a combinatorial method

J. Chem. Phys. **121**, 3745 (2004); 10.1063/1.1765094

State-resolved dynamics of 248 nm methyl-iodide fragmentation on GaAs(110)

J. Chem. Phys. **119**, 10298 (2003); 10.1063/1.1619944

Competition between photochemistry and energy transfer in ultraviolet-excited diazabenzenes. II. Identifying the dominant energy donor for "supercollisions"

J. Chem. Phys. **112**, 5844 (2000); 10.1063/1.481158



Competition between photochemistry and energy transfer in ultraviolet-excited diazabenzenes. I. Photofragmentation studies of pyrazine at 248 nm and 266 nm

Eric T. Sevy,^{a)} Mark A. Muyskens,^{b)} Seth M. Rubin,^{c)} and George W. Flynn
Department of Chemistry and Columbia Radiation Laboratory, Columbia University, New York, New York 10027

James T. Muckerman
Chemistry Department, Brookhaven National Laboratory, Upton, New York 11973-5000

(Received 3 August 1999; accepted 14 December 1999)

The quantum yield for the formation of HCN from the photodissociation of pyrazine excited at 248 nm and 266 nm is determined by IR diode probing of the HCN photoproduct. HCN photoproducts from excited pyrazine are produced via three different dissociation channels, one that is extremely ‘prompt’ and two others that are ‘late.’ The total quantum yield from all reaction channels obtained at low quencher gas pressures, $\phi = 1.3 \pm 0.2$ for 248 nm and 0.5 ± 0.3 for 266 nm, is in agreement with preliminary studies of this process as well as recent molecular beam studies. To investigate if HCN production is the result of pyrazine multiphoton absorption, this photodissociation process has been further studied by observing the HCN quantum yield as a function of total quencher gas pressure (10 mTorr pyrazine, balance SF₆) and as a function of 248 nm laser fluence from 2.8 to 82 mJ/cm². At the highest SF₆ pressures, the HCN quantum yield shows strong positive correlation with laser fluence, indicating that the ‘prompt’ channel is the result of multiphoton absorption; however, at low pressure, the HCN quantum yield is affected little by changing laser fluence, indicating that the majority of the HCN photoproducts at low pressure are produced from pyrazine which has absorbed only one UV photon. At the lowest pressures sampled, HCN produced from the one-photon ‘late’ process accounts for more than 95% of all HCN formed (at low laser fluence). At high pressures the single photon ‘late’ pyrazine dissociation is quenched, and HCN produced at high quencher gas pressures comes only from the multiphoton absorption channel, which can be clearly observed to depend on laser fluence. The HCN quantum yield as a function of laser intensity at high pressure has been fit to a quadratic function that can be used to determine the amount of ‘prompt’ ‘unquenched’ HCN produced from multiphoton photodissociation. Additionally, the information theoretic prior functions for energy disposal in the 248 nm photodissociation of pyrazine to form HCN have also been developed. Prior functions for one, two, and three-photon absorption indicate that only HCN with near room temperature translational energy comes from the one-photon process and that all HCN molecules with large amounts of translational energy are produced by multiphoton processes. Finally, analysis of the quenching data within the context of a strong collision model allows an estimate of the rate constant for HCN production from pyrazine for the major ‘late’ channel, $k_{d1s} = 1.69 \times 10^5 \text{ s}^{-1}$, for 248 nm excitation, and $k_{d1s} = 1.33 \times 10^4 \text{ s}^{-1}$ for 266 nm excitation. After 266 nm excitation, pyrazine produced by the major one-photon channel lives for almost an order of magnitude longer than after 248 nm excitation. © 2000 American Institute of Physics. [S0021-9606(00)00310-X]

I. INTRODUCTION

Over the past several years pyrazine (C₄H₄N₂) has become a very important molecule in the study of collisional energy transfer mechanisms. The favorable spectroscopic characteristics of this molecule, namely its propensity to both fluoresce¹ and phosphoresce^{2,3} at low energies as well as its internal conversion properties, have made it a model system

to study vibrational energy transfer following photoexcitation. The collisional behavior of pyrazine in excited electronic states has been investigated by several groups. Weisman and co-workers²⁻⁵ have probed the collisional relaxation of triplet state pyrazine containing varying amounts of excess vibrational energy, and Rice and co-workers¹ have investigated the intermode vibrational energy transfer in electronically excited singlet pyrazine. Troe and co-workers⁶⁻⁸ using an ultraviolet (UV) absorption technique and Barker and co-workers⁹⁻¹⁵ using time-resolved infrared fluorescence (IRF) studies have amassed an extensive collection of data on the average energy transferred per col-

^{a)}Link Energy Foundation Edwin A. Link Doctoral Fellow.

^{b)}Permanent address: Department of Chemistry and Biochemistry, Calvin College, Grand Rapids, Michigan 49546.

^{c)}Present address: Department of Chemistry, University of California, Berkeley, California 94720.

lision by highly vibrationally excited polyatomics (pyrazine among them) in both the ground and first electronically excited singlet states.

One reason for the substantial interest in pyrazine as a donor in energy transfer studies is the subnanosecond $S_2 \rightarrow T$ intersystem crossing time during which excited pyrazine molecules are quickly converted into vibrationally excited triplet states² with near unity yield. Furthermore, pyrazine subsequently decays quickly almost exclusively by $T \rightarrow S_0$ intersystem crossing producing highly vibrationally excited ground state molecules. On the time scale of single collision events in low pressure gas mixtures (20 mTorr), this intersystem crossing time (approximately 35–50 ns) is much faster than the gas kinetic collision time (4 μ s).^{16–19}

Experiments in this laboratory have focused on using pyrazine as a highly vibrationally excited donor in collisions with simple bath molecules, whose states can be probed with quantum state resolution after the collision event has occurred.^{20–23} The IR diode laser probe technique has been used to measure the nascent rotational and translational excitation in various vibrational states of CO₂ following collisions with vibrationally hot pyrazine.^{24–27} The results from these studies have been used to determine the average energy transferred from pyrazine to CO₂ in a single collision as well as the probability of that collision; further, the data can also be inverted to determine the probability distribution function, $P(E, E')$.^{28,29}

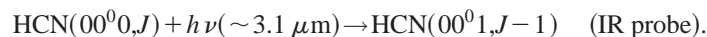
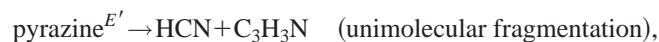
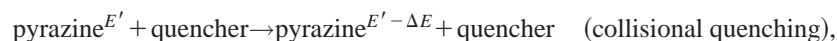
In addition to favorable spectroscopic properties, aromatic molecules have a propensity to dissociate after absorption of UV radiation. Excited benzene, for example, dissociates to form benzyne and other fragments under collision free conditions.^{30–32} Even though in some instances these photoproduct yields are small, in collisional energy transfer studies the extent to which photodecomposition takes place is important, as photochemistry may interfere with interpretation of energy transfer data.¹⁴ Understanding the photochemistry of collisional donor molecules is of particular importance in studies that probe the collision partner, since the bath molecule is blind to the identity of the donor.³³

Nakashima and Yoshihara observed photoproduct formation from benzene at 248 nm. They concluded that the nascent photoproduct in their system resulted largely from multiphoton processes (laser fluences 40–90 mJ/cm²).^{34,35} This is likely the result of the propensity for aromatic molecules to undergo multiphoton absorption. Dissociation following single or multiphoton absorption of UV radiation is not limited to benzene but has also been observed in other aromatic systems.^{11–13}

Over the past several years, the study of pyrazine photochemistry has increased tremendously,^{36–40} including some investigations of pyrazine dissociation after 248 nm absorption to form HCN.^{33,41–43} As noted above, these studies are of particular interest to those who have used pyrazine and other azabenzene as donors in collisional energy transfer studies due to the fact that the photoproducts may provide a second donor for collisional energy transfer clouding interpretation of energy transfer results. Despite the fact that great care was taken to ensure that these pyrazine photofragmentation studies were conducted in the region of linear pyrazine UV absorption, preliminary evidence suggested that some HCN produced in our initial studies of the photodissociation of pyrazine could be the result of multiphoton absorption.⁴³ Therefore, a careful study of the nature of the intensity dependence in the photodissociation of pyrazine is of considerable importance. This is a particularly cogent issue in assessing the relative influence of fast photofragments, which are more likely to be produced by multiphoton absorption than by single photon absorption.

The work described in this paper is the first part of a series of papers focusing attention on the competition between collisional deactivation and decomposition in highly vibrationally excited azabenzene systems. The particular aim of this paper is to determine (1) the lifetime of the excited pyrazine, (2) the dependence of the excited pyrazine lifetime on excitation energy, (3) the influence of collisional energy transfer (quencher gas pressure) on the photoproduct yield, and (4) the characteristics of any multiphoton absorption channels and their effect on the identity of the donor in collisional energy transfer studies. The experiments described are similar to the simple quenching studies performed earlier but investigate fully the intensity dependence of the photofragmentation and quenching processes.⁴³ The implications for these photofragmentation studies for recent energy transfer studies²⁷ are investigated and discussed in the following companion paper.⁴⁴ A third and fourth study will include results from similar investigations of methylpyrazine as well as the di- and tri-substituted methylpyrazines, respectively, which provide insight into the mechanism of the dissociative process.

The first experiment in the present study, a classic quenching investigation in which the HCN quantum yield is measured as a function of quencher gas pressure, was performed to determine the rate constant for the photofragmentation of pyrazine excited at 248 nm and 266 nm. This experiment can be described by the following equations:



Typically, a number of UV laser shots are fired into a closed cell, and after allowing time for the system to reach equilibrium, the HCN population is probed using an IR diode laser. Additionally, CO₂, SF₆, and self-quenching were studied. To determine the influence of pump laser intensity on the photofragmentation process, the intensity of the UV source is also varied and the above described quenching experiment repeated. In these intensity dependent studies, SF₆ was used as the quencher gas, except at the lowest pressure (10 mTorr), where only pyrazine was placed in the cell.

In addition to the quenching studies, information theoretic prior calculations were performed to assess the translational energy probability distribution of HCN photoproducts. These calculations were carried out for several different values of the available energy in order to correlate this distribution with the intensity of the laser pump source in the experiments.

II. EXPERIMENT

The experimental technique for determining quantum yields has been described previously⁴³ and will only be briefly outlined here. A closed Pyrex cell contains gas-phase samples of pyrazine, in some cases mixed with CO₂ or SF₆ quencher gas. Typically, UV laser pulses from either a KrF excimer laser (Lambda Physik EMG 201, 15 ns pulse width) at 248 nm or a frequency-quadrupled Nd-YAG laser (Coherent NY81, 10 ns pulse width) at 266 nm excite the sample at a 1 Hz repetition rate. Studies have shown that pyrazine is extremely susceptible to multiphoton absorption, as will be discussed further in this work; therefore, the UV pulse energy for all data in this paper will be noted in mJ/cm². A series of glass plates set at Brewster's angle are used to attenuate the intensity of the laser where necessary. The collimation of the ≈ 1.5 cm diam beam is adjusted to ensure that the UV beam emerges from the cell unattenuated by the 2.5 cm diam cell aperture, and the beam is turned with a dichroic mirror coated to reflect 248/266 nm wavelengths into a joulemeter detector (Gentec, ED-200), which gives 10.5 mV per mJ response at these wavelengths. Typically, the peak height from the UV signal is determined by averaging 40 laser pulses with a digital oscilloscope (LeCroy 9354A).

The amount of HCN photoproduct is measured by infrared absorption using an IR diode laser technique.⁴⁵ A cw, 3.1 μ m diode laser beam (Mütek) propagates collinearly with the UV beam through the cell and passes through a monochromator (Bausch & Lomb, 0.5 m) to select a single diode laser mode. The diode laser controller (Laser Analytics) modulates the laser frequency over the entire $P22\ 00^00 \rightarrow 00^01$ absorption line of HCN at 1 kHz, and the central diode laser frequency is actively locked using a technique described below. The digital oscilloscope records the amplified signal from a liquid nitrogen cooled InSb detector (Santa Barbara Research Center) placed at the exit slit of the monochromator. A dual-channel acquisition technique²⁷ is used to compensate for diode laser intensity fluctuations, and the result from the summed-average of 1000 sweeps across the absorption line is stored. This signal is usually acquired several minutes after the UV exposure is complete to allow for equilibration of the cell contents. In addition to correcting for

short term fluctuations in laser intensity, variations in diode laser power across the absorption line are corrected for by subtracting the IR signal obtained from an empty cell from the absorption signals obtained from a cell filled with sample.

Active locking of the diode laser frequency to a HCN absorption line is accomplished using a separate HCN reference cell.²⁴ A 30 cm long Pyrex reference cell filled with 1,3,5-triazine is irradiated with 248 nm excimer laser pulses, thus producing HCN via 1,3,5-triazine photodissociation.^{46,47} Approximately 10% of the diode laser beam is directed by a beamsplitter into the reference cell, through a monochromator (Instruments SA Inc., HR-320), and then focused onto an InSb detector (Santa Barbara Research Center) followed by a high gain preamplifier. The HCN IR absorption signal from the reference detector is input to a lock-in amplifier (Princeton Applied Research, Model 117), the output of which is used as an error signal sent to the diode laser controller, thus keeping the diode laser frequency locked to the HCN absorption transition.

To determine the dependence of pyrazine photodissociation on UV pump intensity, the quenching study described above was repeated at multiple UV pump laser intensities. The intensity was changed by varying the number of windows in a Brewster stack. UV intensities from approximately 90 mJ/cm² to 1 mJ/cm² were used. For the SF₆ quenching studies, 10 mTorr of pyrazine was placed into a 10 cm long cell and then various amounts of SF₆ were added. The 10 cm cell was used rather than the 300 cm cell to improve the uniformity of the UV beam (I_0) as a function of cell length (z). Even with gas in the cell, the UV laser intensity at the front of the 10 cm cell is close to the UV laser intensity at the end of the cell; when using a 300 cm cell this is not the case. Additionally, because the excimer beam diverges as a function of cell length (z), for long cells the intensity of the beam decreases significantly as a function of cell length. This is also the reason that SF₆ was used as the quencher in these studies rather than pyrazine itself, to keep the UV exposure down the cell as close to constant as possible. Valves at each end of the cell were closed before the UV laser was fired to provide a more accurate measurement of the cell volume, an important value for the calculation of the total HCN produced in the experiment.

Pyrazine (Aldrich, 99+%) is purified by several freeze (77 K)/pump/thaw cycles; CO₂ (Matheson, 99.995%) and SF₆ (Matheson, 99.995%) are used without further purification. Gas pressures in the cell were monitored with either a 1 Torr (MKS-Baratron 220 C) or a 10 Torr (MKS-Baratron 222BA) capacitance manometer, depending on the pressure range.

III. RESULTS

A. Approach to quantum yield calculations and measurements

The quantum yield, ϕ , for the production of HCN following UV photodissociation is the ratio of the number of HCN molecules produced, N_{HCN} , to the number of photons absorbed, N_{abs} or $\phi = N_{\text{HCN}}/N_{\text{abs}}$.⁴⁸ N_{abs} is calculated

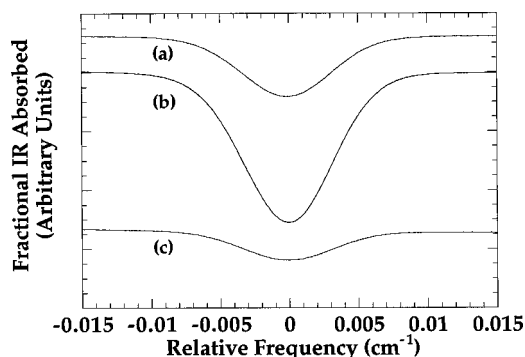


FIG. 1. HCN photoproduct IR absorption signals recorded after pyrazine sample exposure to UV excitation (40 laser shots) for several pyrazine pressures (a) 2 mTorr, (b) 20 mTorr, and (c) 200 mTorr. Signals are the summed average of 1000 sweeps of the diode laser locked to the center of the $P22$ absorption line of HCN ν_3 at 3241.7488 cm^{-1} . The magnitude of the fractional IR absorbed, χ , for each of these pressures is (a) 0.021, (b) 0.051, and (c) 0.010. The full-width at half-maximum (FWHM) for each plot is essentially the same, $0.0077 \pm 0.0001\text{ cm}^{-1}$ which corresponds to a room temperature Doppler broadened absorption line of $T = 297 \pm 8\text{ K}$. Measurements were conducted at a UV laser fluence of 9.5 mJ/cm^2 .

from the total UV energy absorbed, E_{abs} , with $N_{\text{abs}} = E_{\text{abs}}(\lambda/hc)$, where λ is wavelength, h is Planck's constant, and c is the speed of light. $E_{\text{abs}} = E_0 - E$ is measured as the difference between the energy emerging from an empty cell, E_0 , and filled cell, E , using a calibrated joulemeter.

The number of HCN molecules produced is determined by measuring IR absorption on the ν_3 , $P22$ transition of HCN ($\nu = 3241.7488\text{ cm}^{-1}$). (It should be noted that the HCN population in $J=22$ is very sensitive to temperature, which is a potential source of error in the measurement of the HCN concentration and consequently ϕ .) The dual-channel acquisition technique yields the fractional IR absorption, χ , which is defined by $\chi = \Delta I/I$, where $I = I_0 - \Delta I$. Figure 1 shows the fractional IR absorption by HCN resulting from 248 nm photodissociation at three different initial pyrazine pressures. The desired quantity for calculating absorbance is $I/I_0 = 1/(1 + |\chi|)$, where the absolute value of χ is used simply because the negatively-biased IR detector yields χ with negative values. The number of HCN molecules is then $N_{\text{HCN}} = -\ln(1/(1 + |\chi|))V/\sigma l$,⁴⁹ where V is the vacuum manifold volume consisting mostly of the cell volume of length l , and σ is the absorption cross section for this IR transition. Assuming a Doppler lineshape function for this absorption line and using a literature value for the HCN $P22$ line strength $S = 3.88 \times 10^{-20}\text{ cm}^{-1}(\text{cm}^2/\text{molecule})$,⁵⁰ we calculate $\sigma = 4.71 \times 10^{-18}\text{ cm}^2$. Figure 1 shows clearly that the absorbed IR radiation fails to increase continually with increasing pyrazine pressure. The number of UV photons absorbed continues to increase (as long as the cell is not opaque to the laser beam) with increasing pyrazine pressure; therefore, the quantum yield falls off with increasing pyrazine pressure. The quantum yields for the pressures shown in Fig. 1 are 1.16 ± 0.24 , 0.54 ± 0.10 , and 0.10 ± 0.02 for 2, 20, and 200 mTorr, respectively.

B. Self-quenching of excited pyrazine

The dramatic decline in the HCN quantum yield from UV-excited pyrazine as a function of increasing pressure

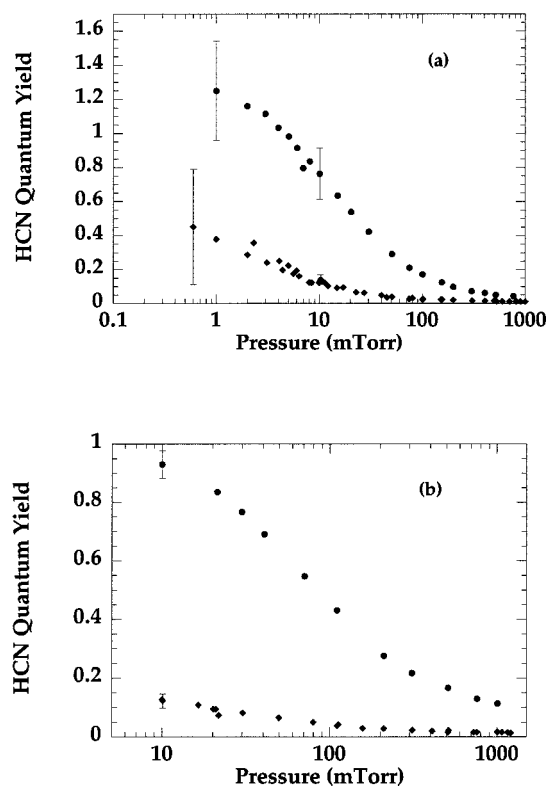


FIG. 2. Quenching curves showing the HCN quantum yield dependence on pressure. (a) Displays the collisional quenching of excited pyrazine by unexcited pyrazine. The circles represent the HCN quantum yield after 248 nm excitation, while the diamonds represent the data after 266 nm excitation. (b) CO_2 -quenching curves for pyrazine showing the HCN quantum yield dependence on total pressure (in a mixture of 10 mTorr of pyrazine with balance CO_2); the circles are for 248 nm excitation, and the diamonds are for 266 nm excitation. Quantum yield measurements obtained for 248 nm and 266 nm excitation were conducted at UV laser fluences of 9.5 mJ/cm^2 and 5.0 mJ/cm^2 , respectively.

over three decades is shown in Fig. 2(a). The quantum yields from 266 nm excitation are significantly less than the 248 nm values at the same pressures. Note that the quantum yield falls to less than half of the maximum value found at the lowest pressure within the first decade (1–10 mTorr). The significant quenching occurring at these low pressures suggests that the photodissociation process is quite slow, occurring on a microsecond time scale. Another feature of these quenching curves is that the quantum yield in the limit of high pressure appears to level off at some small nonzero value. This is the clearest evidence of a second, ‘‘prompt’’ HCN production channel that is, therefore, less easily quenched. At higher pressures this channel too will eventually be quenched. There is strong evidence to suggest that this second, fast HCN product channel is the result of multiphoton absorption by pyrazine. This is discussed at length below.

An interesting feature of Fig. 2(a) is that the quantum yield for 248 nm excitation of pyrazine in the low pressure limit exceeds unity below about 5 mTorr. Although quantum yield measurements in this low pressure regime are subject to relatively large error, this is not necessarily an unrealistic result because pyrazine may fragment in such a way that two HCN molecules and acetylene are formed,



Strong acetylene absorption lines exist in the frequency range of the diode laser used to probe HCN, allowing for a measurement of the acetylene quantum yield for 248 nm excitation of pyrazine. These results show a maximum C_2H_2 quantum yield of no more than 0.03, indicating a HCN quantum yield of 0.06 from this channel. A self-quenching curve for the acetylene quantum yield as a function of pressure, analogous to Fig. 2(a), indicates that the quenching of this acetylene producing channel occurs at an even lower pressure than for the dominant HCN product channel.

This “extra” HCN which is produced via “Channel 2” easily accounts for the greater than 1 quantum yield. At the lowest pressures, the maximum HCN quantum yield is approximately 1.2 ± 0.15 which is within error limits of the theoretical maximum quantum yield of 1.06 determined by adding the maximum of $\phi = 1.0$ from the 1 HCN channel and $\phi = 0.06$ from the 2 HCN channel. Sources of uncertainty are discussed below.

C. CO_2 quenching of excited diazabenzenes

The dependence of the HCN quantum yield on added CO_2 acting as a quencher is displayed in Fig. 2(b), where the total pressure is the result of a mixture of 10 mTorr of pyrazine with various amounts of CO_2 (e.g., 20 mTorr total pressure with equal amounts of pyrazine and CO_2). The overall features of decreasing quantum yield and apparent nonzero quantum yield at high pressure seen in Fig. 2(a) are present here as well. The quantum yield at 10 mTorr of pure pyrazine agrees reasonably well with corresponding data in Fig. 2(a); therefore, these curves clearly show the relative quenching effectiveness of CO_2 vs pyrazine. In general, the CO_2 quenching experiments show a much smaller effect on the HCN quantum yield over a given pressure range, say 10–100 mTorr, than for the self-quenching studies, a clear indication that CO_2 is a less efficient quencher than unexcited pyrazine. The collisional deactivation experiments of both Barker⁵¹ and Troe⁸ have convincingly demonstrated that the quenching efficiencies of highly excited molecules scale roughly with the “complexity” of the bath gas. Thus, our observation that pyrazine is a better quencher than CO_2 is not surprising. Additionally, the 248 nm data from Figs. 2(a) and 2(b) are in reasonable agreement with those obtained in previous experiments.⁴³

D. UV absorbance

The UV absorbance $A_{\text{UV}} = -\log(I/I_0)$ of pyrazine is found to be linear with pressure at $I_0 = 9.5 \text{ mJ/cm}^2$. Figure 3 shows that the pressure dependence of the UV absorption for pyrazine at 248 nm is linear over a range of more than two orders of magnitude, and similar behavior is observed at 266 nm.⁵² Beer’s Law relates the slope of the plots shown here to the molar absorptivity, ϵ , by $A = (\epsilon/lRT)p$, where concentration is expressed in terms of pressure p , ($n/V = p/RT$), l is the cell path length, R is the gas law constant, and T is the temperature in Kelvin. Based on this data, the molar absorp-

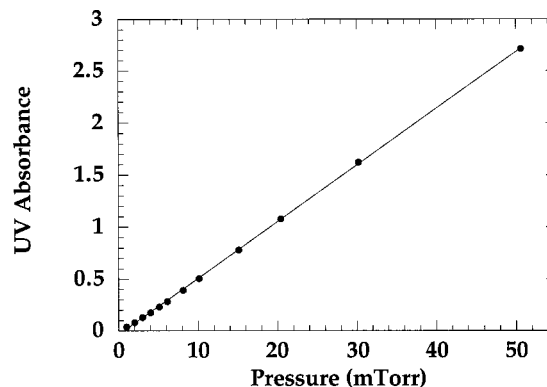


FIG. 3. UV absorbance of pyrazine at 248 nm plotted as a function of pressure. The line is a linear least squares fit to the data and shows good adherence to Beer’s Law for UV absorption over a pressure range of more than two orders of magnitude. Measurements were conducted at an UV laser fluence of 9.5 mJ/cm^2 .

tivity of pyrazine at 248 nm is $3.2 \pm 0.1 \times 10^3 \text{ (L/mol) cm}^{-1}$. These absorption studies are in reasonable agreement with other measurements of the absorption coefficient of pyrazine by Bolovinos and co-workers,⁵³ $4 \pm 0.3 \times 10^3 \text{ (L/mol) cm}^{-1}$, and those performed in our lab using a UV/Vis spectrometer, $3.9 \pm 0.4 \times 10^3 \text{ (L/mol) cm}^{-1}$. Additionally, the UV absorbance has been found to be a linear function of laser intensity over the range of 0–30 mJ/cm^2 . The basic assumption of Beer’s Law, that absorbed light intensity ΔI is directly proportional to the incident light intensity I_0 , is only appropriate if there is no multiphoton absorption and thus adherence to Beer’s Law for UV absorption of pyrazine in these studies might lead one to believe that there is no multiphoton absorption. However, as seen in Fig. 4, the HCN quantum yield after 248 nm excitation of pyrazine is intensity dependent at high quencher gas pressure. These intensity dependent studies, described in detail in the next section, show that pyrazine is sensitive to multiphoton absorption. For laser intensities $< 30 \text{ mJ/cm}^2$ multiphoton absorption is very small compared

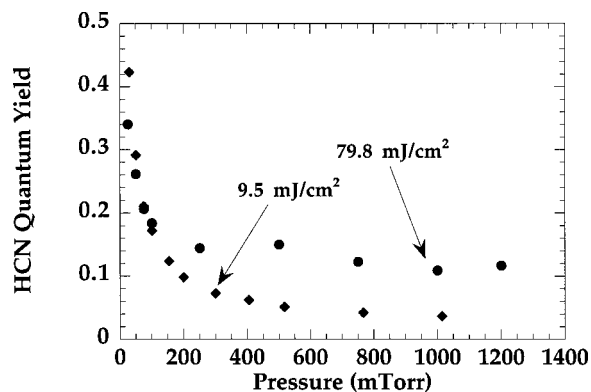


FIG. 4. Plots of the HCN quantum yield as a function of pyrazine pressure at two different UV excitation laser intensities. The circles represent data for a 248 nm pump laser excitation fluence of 79.8 mJ/cm^2 while the diamonds represent data from a 248 nm pump laser fluence of 9.5 mJ/cm^2 . Although the HCN quantum yield at low pressure appears to be independent of pump laser intensity, the high pressure tail is markedly different for the two sets of data indicating that the photodissociation process is intensity dependent.

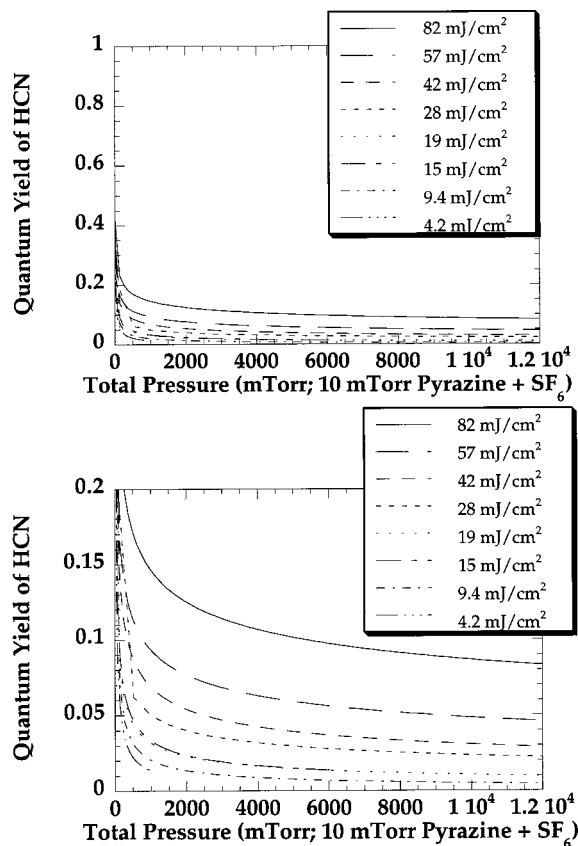


FIG. 5. Pyrazine-SF₆ quenching curves showing the HCN quantum yield [$\phi_{\text{HCN}} = ([\text{HCN}]/N_{\text{hv}})$] dependence on pressure and UV laser intensity. The pressure is a combination of 10 mTorr of pyrazine with the balance SF₆ ranging from 0 to 12 000 mTorr. The various curves arise from a difference in UV laser fluence measured in mJ/cm². (a) Shows the curves over the entire data range, while (b) is an enlargement, only showing the data obtained for quantum yields less than 0.2. The lines are the result of a nonlinear least squares fit to the data.

with one-photon absorption; therefore, deviations from linear absorption as either a function of pressure or laser intensity in this range (<30 mJ/cm²) are difficult to observe in a direct absorption measurement.

E. Intensity dependent SF₆-quenching of 248 nm excited pyrazine

The HCN quantum yield as a function of total gas pressure (10 mTorr pyrazine, balance SF₆) for eight different UV laser intensities ranging from 82 mJ/cm² to 2.8 mJ/cm² is shown in Fig. 5. As seen in previous quenching results for pyrazine photodissociation,⁴³ these quenching curves show a dramatic decline in the HCN quantum yield from 248 nm excited pyrazine as a function of increasing pressure. While the decline in HCN quantum yield is very rapid in the pressure range from 0 to 50 mTorr the decline is much less pronounced over the remainder of the pressure range. Note further that in the high pressure limit the quantum yield roughly levels off to some nonzero value. Each quenching curve individually shows this trend, i.e., a rapid decrease in HCN quantum yield as the pressure is initially increased and then a leveling off and approach to some nonzero value. That

significant quenching occurs at low pressures suggests, as reported previously, that the majority of the HCN formed in the photodissociation process is produced quite slowly (microsecond time scale).⁴³ The nonzero quantum yields seen at high quencher gas pressures are associated with a different, faster HCN production channel that is, therefore, less easily quenched. As can be seen clearly in Fig. 5(b), a blow up of the high pressure region, the asymptotic value of the high pressure quantum yield also decreases as the excitation laser intensity is decreased. Furthermore, the general shape of the various quenching curves is essentially the same (only lowered by some factor as the intensity decreases).

There are two significant qualitative features that are obvious from inspection of the quenching curves. The first is that the HCN quantum yields do not appear to be substantially affected by the variation in 248 nm excitation intensity at low quencher gas pressure. This is due to the fact that the yield from the multiphoton channel is only a small fraction (2%–7% over the fluence range studied) of the total yield in this pressure range. The other key feature is a uniform decrease in the nonzero high pressure tail indicating that the high pressure quantum yield steadily decreases as UV intensity is decreased.

As seen in the CO₂ quenching experiments, the quantum yield in the SF₆ quenching studies at $p_{\text{tot}}=10$ mTorr ($p_{\text{pyr}}=10$ mTorr, $p_{\text{SF}_6}=0$ mTorr) agrees reasonably well with corresponding data in Fig. 1 of Ref. 43 and Fig. 2 of this study. In general, the SF₆ quenching is less efficient than pyrazine self-quenching over a given pressure range; however, SF₆ quenching is much more effective than CO₂ quenching. Again, this is as expected based on the collisional deactivation experiments of Barker⁵¹ and Troe⁸ discussed above. Pyrazine, being the most “complex” of the three molecules, is the most efficient quencher; SF₆ is less efficient, and CO₂, being the least “complex,” is the least effective at quenching the reaction. Additionally, these results are in good agreement with quenching studies of *T*₁ pyrazine, which indicate that quencher efficiencies vary such that *S*₀ pyrazine is most efficient, followed by SF₆ and CO₂ in that order.⁹

F. Information theoretic prior calculations

Here, the information theoretic prior functions for energy disposal in hydrogen cyanide (HCN) and some product with the chemical formula C₃H₃N resulting from the 248 nm photodissociation of pyrazine are developed. This treatment makes use of the general formulas of Ref. 54, and equations derived below follow the methods outlined therein.

Among the cases treated in Ref. 54 is that of unimolecular decomposition yielding a linear triatomic molecule and a general nonlinear molecule. The special features of this case are: (1) that the linear triatomic molecule has only *two* rotational degrees of freedom and $3n-5=4$ vibrational degrees of freedom and (2) the general nonlinear molecule, in the spherical top approximation, has rotational levels that are $(2J_g+1)^2$ degenerate. Equation (32) of Ref. 54 shows that the multidimensional prior function for this case is

$$\rho^0(f_1^t, f_{2a}^t, f_{2b}^t, f_3^t, f_R^t, f_1^g, \dots, f_s^g, f_R^g; E) = \frac{2^2}{\pi} (s+7)! (f_R^g)^{1/2} [1 - f_1^t - f_1^g]^{1/2}, \quad (1)$$

where f represents a fraction of the *total* available energy; the superscript t or g indicates the “triatomic” or “general” fragment, respectively; $s = 3n - 6$ is the number of vibrational modes in the general molecule; the subscript $1, \dots, s$, represents vibrational energy in the indicated mode; the subscript R , rotational energy of the fragment, and the subscript I , internal energy in the fragment. For the case of pyrazine photodissociation, the C_3H_3N fragment contains 7 atoms, thus $s = 15$.

Following Eq. (35) of Ref. 54, the prior fraction of the total available energy, appearing as vibrational energy in the various modes of the linear triatomic molecule (HCN), is

$$\rho^0(f_{1;3}^t) = (s+7)(1-f_{1;3}^t)^{s+6} \quad (2)$$

for nondegenerate modes ν_1 and ν_3 and

$$\rho^0(f_2^t) = (s+7)(s+6)f_2^t(1-f_2^t)^{s+5} \quad (3)$$

for the doubly-degenerate ν_2 mode. The prior total vibrational energy of the HCN fragment is

$$\rho^0(f_V^t) = \frac{(s+7)(s+6)(s+5)(s+4)}{6} (f_V^t)^3 (1-f_V^t)^{s+3}, \quad (4)$$

where $f_V^t = f_1^t + f_{2a}^t + f_{2b}^t + f_3^t$. The prior rotational energy of the HCN fragment is identical in form to Eq. (2),

$$\rho^0(f_R^t) = (s+7)(1-f_R^t)^{s+6}, \quad (5)$$

and the prior internal energy of the HCN fragment is

$$\rho^0(f_I^t) = \frac{(s+7)(s+6)(s+5)(s+4)(s+3)}{24} (f_I^t)^4 (1-f_I^t)^{s+2}, \quad (6)$$

where $f_I^t = f_V^t + f_R^t$. Defining $f_T = 1 - f_I^t + f_1^g$, the prior for the fraction of available energy appearing as relative translational energy becomes

$$\rho^0(f_T) = \frac{(s+8)}{\Gamma(\frac{3}{2}) + \Gamma(s + \frac{13}{2})} (f_T)^{1/2} (1-f_T)^{s+11/2}, \quad (7)$$

where Γ is the gamma function. The prior distributions for $f_1^t, f_2^t, f_3^t, f_V^t, f_R^t$, and f_I^t are shown in Fig. 6. Average values of f_i^t for $i = 1, 2, 3, R, V$, and f_T calculated using

$$\langle f_i \rangle = \int_0^1 f_i \rho^0(f_i) df_i \quad (8)$$

and Eqs. (2)–(7) are consistent with the equipartition theorem and are listed in Table I. The sum of f_1^t and f_T , from Table I reveals that the prior average fraction of the available energy appearing as internal energy in the C_3H_3N fragment is 0.717 392, since

$$1 = f_1^g + f_1^t + f_T. \quad (9)$$

Of this, according to the equipartition theorem, 0.652 174 appears as total vibrational energy and 0.065 217 as rotational energy of this larger fragment.

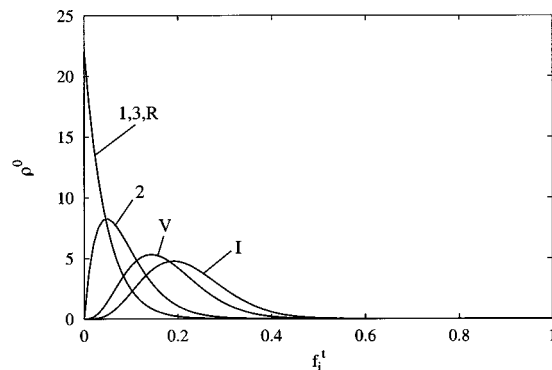


FIG. 6. Single-variable prior probability density functions $\rho^0(f_i^t)$, for the HCN- C_3H_3N system. The curves are labeled by $i = 1, 2, 3, R, V$, and I . 1, 2, and 3 correspond to the three vibrational modes of HCN and R, V , and I correspond to the rotational, total vibrational, and total internal degrees of freedom respectively.

Table I also contains the average available energy, $\langle E_{avl} \rangle$, in each HCN degree of freedom after photodissociation. Although no *a priori* information about the specifics of the general product fragments in the photodissociation is required to calculate the prior functions, other than the number of vibrational degrees of freedom, to determine the energy available to the photofragments after dissociation, the C_3H_3N product must be known. The available energy after dissociation can be calculated using

$$E_{avl} = E_{int} + E_{hv} - \Delta H_r, \quad (10)$$

where E_{hv} is the energy of the absorbed photon, ΔH_r is the enthalpy of reaction to form HCN and the specific C_3H_3N product molecule, and E_{int} is the internal energy of pyrazine before absorption, given by

TABLE I. Prior average fractions^a of available energy and average available energy in various HCN degrees of freedom from the photodissociation of pyrazine.^b

HCN degree(s) of freedom	$\langle f_i^t \rangle^a$	$\langle E_{avl} \rangle^c$	$\langle E_{avl} \rangle^d$	$\langle E_{avl} \rangle^e$
ν_1	0.043 478	1.77	6.78	11.8
ν_2	0.086 957	3.54	13.57	23.6
ν_3	0.043 478	1.77	6.78	11.8
total vibration (V)	0.173 913	7.08	27.1	47.2
rotation (R)	0.043 478	1.77	6.78	11.8
total internal (I)	0.217 391	8.85	33.9	59.0
relative translation (T)	0.065 217	2.65	10.2	17.7

^aPrior average fraction, $\langle f_i^t \rangle$, of available energy calculated from Eq. (8).

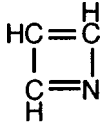
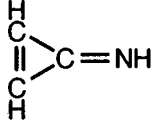
^b $\langle E_{avl} \rangle = E_{avl} \langle f_i^t \rangle$. Energies are given in kcal/mol. E_{avl} from Table II assuming *N*-ethynyl-methylimine as the C_3H_3N product.

^cAverage energy after a one-photon dissociation process. $E_{avl} = 40.7$ kcal/mol.

^dAverage energy after a two-photon dissociation process. $E_{avl} = 156.0$ kcal/mol.

^eAverage energy after a three-photon dissociation process. $E_{avl} = 271.2$ kcal/mol.

TABLE II. Heats of formation and values for available energy after photodissociation for various C₃H₃N reaction products from the 248 nm photodissociation of pyrazine to form HCN.^{a,b,c}

Product	ΔH_f (298 K) ^d	ΔH_r ^e	$1-h\nu E_{avl}$ ^f	$2-h\nu E_{avl}$ ^f	$3-h\nu E_{avl}$ ^f
 azete	(110.7)	(96.1)	20.1	135.4	250.6
 cyclopropene-1-imine	(97.8)	(83.2)	32.9	148.3	263.5
HC≡C—N=CH ₂ <i>N</i> -ethynyl-methylimine	(90.1)	(75.5)	40.7	156.0	271.2
HC≡C—C(=NH) H propargylimine	(82.7)	(68.1)	48.1	163.4	278.6
HC≡CH HC≡N acetylene+HCN	[86.8]	[72.2]	44.0	159.0	274.5
H ₂ C=C≡N H acrylonitrile	(48.1) [43.2]	(33.7) [28.6]	82.5 87.6	197.8 202.9	313.0 318.1

^aAll values are given in kcal/mol.

^bValues in parentheses are based on *ab initio* calculations from Ref. 57.

^cValues in brackets are from Ref. 56.

^dEnthalpy of formation to produce HCN and C₃H₃N product(s) at 298 K.

^eReaction enthalpy used to calculate the energy available to pyrazine photoproducts after 248 nm dissociation.

^fEnergy available, E_{avl} , to the photoproducts following dissociation of a pyrazine molecule which has absorbed 1-, 2-, or 3- 248 nm UV photons calculated according to Eq. (10).

$$E_{int} = \sum_{i=1}^{24} \frac{h\nu_i}{\exp(h\nu_i/kT) - 1}. \quad (11)$$

Using the vibrational frequencies for pyrazine from Ref. 55, $E_{int} = 317 \text{ cm}^{-1}$. Table II contains values for the enthalpy of formation (ΔH_f), enthalpy of reaction (ΔH_r), and available energy (E_{avl}) after a one, two, and three-photon photodissociation of pyrazine to produce HCN and several possible C₃H₃N products. The enthalpies are either experimentally measured⁵⁶ or the result of *ab initio* calculations.⁵⁷ While there are several possibilities for the C₃H₃N photoproduct, *N*-ethynyl-methylimine has been assumed since it is the simplest to form. Only two pyrazine bonds are broken to produce HCN and this product and no new bonds are formed. Of the other possible C₃H₃N products, the first two possible products, azete and cyclopropene-1-imine, were not used because of the highly constrained product forms, and the final possible product was eliminated because several rearrangement steps are necessary to produce acrylonitrile from pyrazine. The three remaining possibilities have very similar enthalpies of formation and therefore, very similar amounts of available energy.

The predicted prior distributions for the translational energy of HCN, f_T , are shown in Fig. 7 for various amounts of available energy corresponding to three, two, and one-photon absorption before dissociation and the production of HCN and *N*-ethynyl-methylimine in the dissociation process.

IV. DISCUSSION

The experiments in this paper have been designed to determine two facts with regard to the photodissociation of pyrazine. The first is the lifetime of the highly vibrationally excited pyrazine molecule before dissociation to form HCN and other fragments. The second issue is the origin of the “prompt” “unquenched” dissociation channel and the relationship of this “prompt” HCN to translationally fast photoproducts. The second question is addressed first using two sets of data, the intensity dependent results and the surprisal analysis. The information obtained in answering this question will then be used, in part, in a detailed analysis of the photodissociation rates.

A. “Prompt” dissociation, multiphoton absorption, and fast HCN

Several features of the 248 nm intensity dependent studies deserve further discussion. Figure 8(a) shows the HCN quantum yield at 10 mTorr total cell pressure as a function of UV laser intensity. Based on this, one might be led to assume that HCN production is not UV laser intensity dependent. In reality one of the two HCN product channels is intensity dependent, as will become clear at higher quencher gas pressures; however, at these lowest pressures, the intensity dependence is not easily observed because the dominant HCN production channel at 10 mTorr is a one-photon process. As

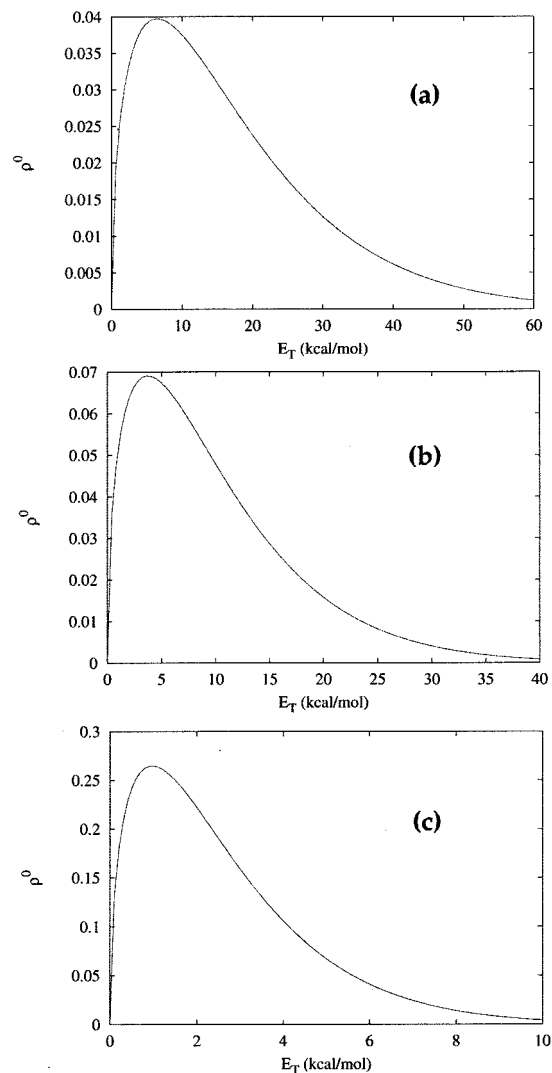


FIG. 7. Calculated single variable prior probability density functions for the one, two, and three-photon dissociation of pyrazine by 248 nm UV excitation. For each curve, the probability density of HCN is plotted as a function of translational energy in kcal/mol. (a) Shows the theoretic prior function for HCN photoproduct having $E_{av1}=271.2$ kcal/mol (i.e., the energy available after dissociation). This corresponds to pyrazine absorbing 3–248 nm UV photons before dissociation. (b) Shows the theoretic prior function for an HCN photoproduct having $E_{av1}=156.0$ kcal/mol (two-photon excitation of pyrazine), and (c) is the prior function for one-photon excitation of pyrazine with $E_{av1}=40.7$ kcal/mol.

as a result, the intensity dependence associated with a multiphoton process is not detectable above the error limits associated with the quantum yield measurements. The largest error, of course, comes at the lowest pressures. At these very low pressures, because the quantum yield varies rapidly with small changes in pressure, a small error in measuring the pressure can account for the scatter in the quantum yield in this range. A straight line with essentially zero slope can be drawn through the points in Fig. 8(a) indicating that the dominant quantum yield channel is independent of laser fluence at this pressure (10 mTorr pure pyrazine). At these lowest pressures, the quantum yield is dominated by a single photon photodissociation process. The probability of any

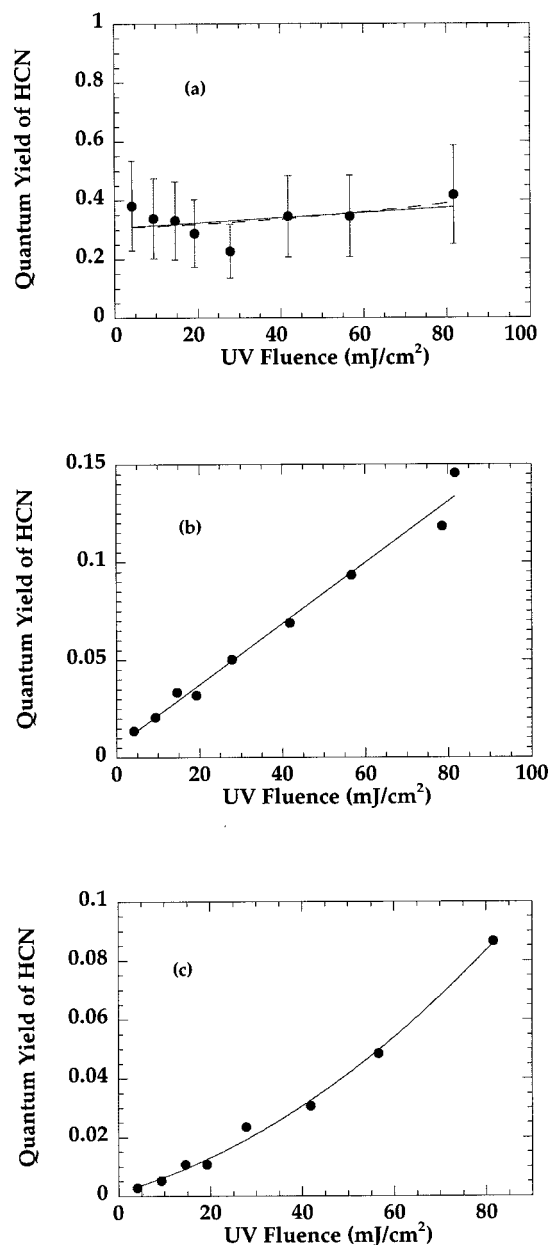


FIG. 8. Cross sections of the data shown in Fig. 5. In all cases the quantum yield of HCN is plotted as a function of 248 nm UV laser fluence in mJ/cm². (a) Shows the fluence dependent data at a total pressure of 10 mTorr (pure pyrazine). The quantum yield is essentially constant, within error limits, showing that the primary photodissociation channel at low pressures is largely insensitive to laser fluence. The solid line is the best linear least squares fit to the data while the dashed line shows the predicted influence of changing the laser fluence based on Eq. (12). (b) Displays the intensity dependent data at a total gas pressure of 1000 mTorr (10 mTorr pyrazine+990 mTorr SF₆). The circles are the measured quantum yields while the straight line is a linear least-squares fit to the data. (c) Shows the intensity dependent data at 10 Torr total pressure (10 mTorr pyrazine+9990 mTorr SF₆). The circles are the measured quantum yields at 10 Torr and the line is the best fit to a quadratic function [Eq. (12)].

multiphoton process, which must also exist at this pressure, is expected to be much smaller than that of the single photon process.

As total gas pressure is increased, the effects of pump laser intensity become clear. At a total gas pressure of 1000 mTorr, as shown in Fig. 8(b), a positive linear correlation

between quantum yield and pump laser intensity is observed. As total gas pressure is continually increased, HCN is no longer produced via the “late” channel, which is quenched due to the increased gas pressure. The HCN from the prompt channel dominates in this pressure regime and the quantum yield is easily seen to be dependent on laser fluence. Figure 8(c) shows the HCN quantum yield as a function of laser fluence arising from a total gas mixture of 10 Torr (10 mTorr pyrazine, balance SF₆). This curve provides strong evidence that a second, “prompt” photodissociation channel exists and further indicates that the HCN from this channel depends on excitation laser fluence and is, hence, the result of a multiphoton process.

Figure 8(c) provides a means of accurately determining the amount of HCN produced from the prompt multiphoton channel at a specific laser intensity, since all pyrazine that would produce HCN via a one-photon process has already been quenched in this pressure range. The HCN quantum yields (Φ_{HCN}) as a function of UV laser intensity (I_{laser} given in mJ/cm²) at a total gas pressure of 10 Torr can be fit to a quadratic function,

$$\Phi_{\text{HCN}} = (4.4 \times 10^{-4})I_{\text{laser}} + (7.3 \times 10^{-6})I_{\text{laser}}^2 \quad (12)$$

While at modest laser intensities (30 mJ/cm²) the multiphoton quantum yield is small ($\phi \sim 0.02$),⁴³ as the laser fluence increases this channel becomes more dominant. At laser fluences of 200 mJ/cm², Eq. (12) predicts a multiphoton HCN quantum yield of approximately 0.40, making the multiphoton processes much more easily detectable, even at low quencher gas pressures. This observation is in agreement with intensity studies performed by Chesko and Lee⁴² who observed that multiphoton effects were easily detected at these laser intensities.

Several features of the surprisal analysis are also worthy of further note. First, the three translational prior functions agree extremely well with recent molecular beam studies of the 248 nm photodissociation of pyrazine to form HCN.⁴¹ In the molecular beam experiments three different HCN “channels,” 27-A, 27-B, and 27-C, have been observed which correlate very well with these predicted three, two, and one-photon prior functions, respectively.

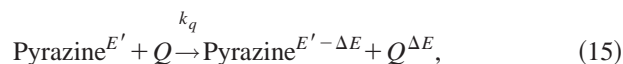
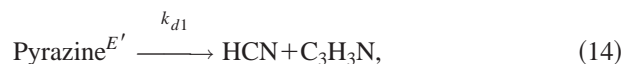
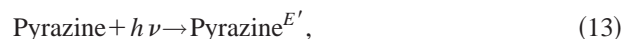
A second key feature of the surprisal analysis is that the high velocity HCN is predicted to be primarily associated with the multiphoton channels. In the case of one-photon absorption where only 40.7 kcal/mol of energy is available to the photoproducts after dissociation, essentially all the HCN molecules have less than 6 kcal/mol of translational energy, with an average relative translational energy of 2.65 kcal/mol. This is only about four times the amount of translational energy available at room temperature (RT=0.596 kcal/mol, $T=300$ K). In the case of HCN produced after the absorption of two-photons [Fig. 7(b)], however, a maximum translational energy release of about 40 kcal/mol with an average of 10.2 kcal/mol is calculated, and the three-photon process produces HCN with even greater translational energies [see Fig. 7(a)]. In this instance, as seen in Fig. 7(a), HCN photoproducts possess a maximum translational energy of roughly 60 kcal/mol and an average of 17.7 kcal/mol.

According to this surprisal analysis, most of the high velocity HCN produced in the photodissociation of pyrazine at 248 nm results from multiphoton absorption.

These two pieces of data taken together provide key information about the photodissociation of pyrazine to form HCN. The intensity dependent studies show that the “prompt” “unquenched” channel is the result of multiphoton absorption. Additionally, the surprisal analysis shows that the HCN photoproducts with high velocity are associated primarily with two and three-photon absorption. Thus, the HCN photoproducts with large amounts of translational energy come from the “prompt” “unquenched” dissociation channel. As shown below, a quantitative analysis of the data indicates that the multiphoton channels constitute less than 3% of the photoproducts at low to moderate UV laser fluence.

B. Detailed photodissociation kinetics

The quenching data can be used to estimate the first order rate constant for the photoproduction of HCN and hence the lifetime of the hot donor. The simplest approach towards a kinetic analysis of the data ignores any additional fragmentation channels such as the multiphoton channel or one which would produce 2 HCN molecules and assumes only the dominant decomposition channel producing a single HCN. While this analysis is only strictly valid for systems at the lowest laser intensities, it provides a good starting point for the analysis. This scheme is described by



where Q is the quencher gas species (either Pyrazine, SF₆, or CO₂) and E' is the energy of the excited donor molecule. Note that this is essentially the Lindemann mechanism for thermal unimolecular reactions, where optical excitation rather than collisional activation has been used to create the highly excited molecules.

In terms of Eqs. (14) and (15), the strong collision model states that Pyrazine ^{$E' - \Delta E$} is not susceptible to dissociation, where $E' - \Delta E$ is less than E_0 , the critical energy needed for dissociation. Furthermore, k_q is the gas kinetic collision rate constant, and the mean time between collisions is $t_{\text{coll}} = 1/k_q[Q]$. Using this simplest model, the kinetics (for long times after pyrazine excitation) predict a linear relationship that relates the HCN quantum yield, ϕ , to the mean collision time by

$$\frac{1}{\phi} = \frac{N_{\text{abs}}}{N_{\text{HCN}}} = \frac{k_q[Q] + k_{d1}}{k_{d1}} = \frac{t_d}{t_{\text{coll}}} + 1, \quad (16)$$

where $t_d = 1/k_{d1}$ is the dissociation lifetime and $t_{\text{coll}} = 1/k_q[Q]$ is the mean collision time. The slope of a plot of $1/\phi$ vs $1/t_{\text{coll}}$ yields the dissociation lifetime, t_d , with an

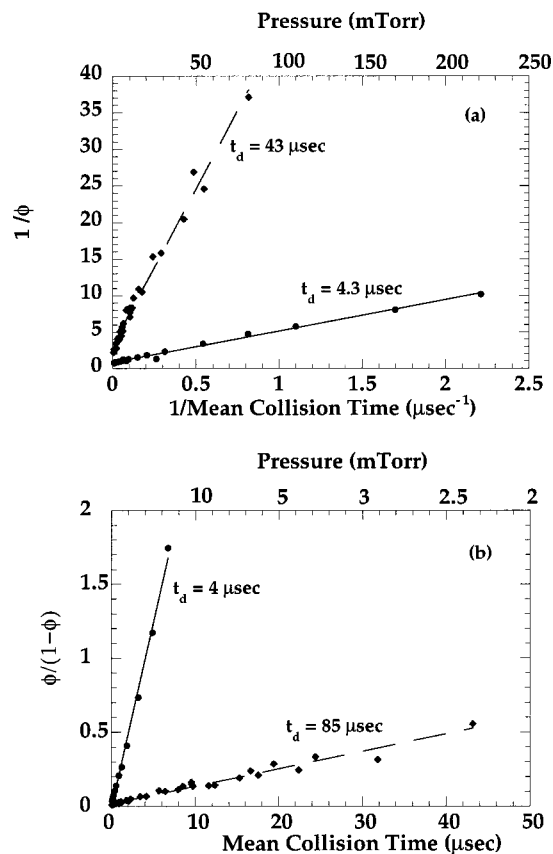


FIG. 9. Quantum yield (ϕ) measurements for excited pyrazine quenched by unexcited pyrazine are presented using a strong collision model. Yields for 248 nm excitation are displayed by circles while 266 nm excitation is represented with diamonds. The lines are best linear least-squares fits to the data. (a) Plots of the inverse HCN quantum yield ($1/\phi$) vs inverse mean collision time ($1/t_{\text{coll}}$). The slope, as predicted by Eq. (16) provides a value of $2.3 \times 10^5 \text{ s}^{-1}$ and $2.3 \times 10^4 \text{ s}^{-1}$ (248 and 266 nm excitation, respectively) for the first-order photodissociation rate constant. (b) Displays $\phi/1-\phi$ as a function of mean collision time (t_{coll}). In this case, as determined by Eq. (17), the slope provides values of $2.5 \times 10^5 \text{ s}^{-1}$ and $1.2 \times 10^4 \text{ s}^{-1}$ (248 and 266 nm excitation, respectively) for the first-order photodissociation rate constant. Differences in the values of t_d derived from (a) vs (b) demonstrate the failings of a model that incorporates only one possible photodissociation channel.

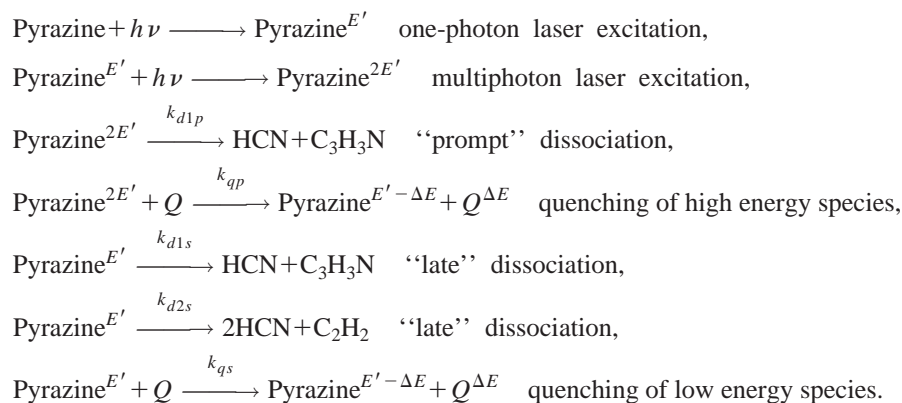
intercept of unity. Applying this model to the pyrazine data gives the linear fits shown in Fig. 9(a). The lifetime for pyrazine with 37910 cm^{-1} of internal energy, $t_d = 43 \mu\text{s}$, is an order of magnitude greater than that for the same molecule with 40640 cm^{-1} internal energy, $t_d = 4.3 \mu\text{s}$. Keeping in mind that the figure displays inverse mean collision time, the linear behavior for this data is found over the range $t_{\text{coll}} = 0.45\text{--}109 \mu\text{s}$ for 248 nm excitation and $t_{\text{coll}} = 1.2\text{--}160 \mu\text{s}$ for 266 nm excitation. An alternative arrangement of Eq. (16) which is directly proportional to the mean collision time is

$$\frac{\phi}{1-\phi} = \frac{t_{\text{coll}}}{t_d}. \quad (17)$$

In this case, the slope of a plot of $(\phi/1-\phi)$ vs t_{coll} yields the

inverse of the dissociation lifetime, $1/t_d$. Figure 9(b) shows a plot of the experimental data giving a value of $t_d = 85 \mu\text{s}$ for 266 nm excitation and $4 \mu\text{s}$ for 248 nm excitation. The fit of the data to Eq. (17) is linear over the range $t_{\text{coll}} = 0.09\text{--}6.7 \mu\text{s}$ for 248 nm and $t_{\text{coll}} = 0.08\text{--}43 \mu\text{s}$ for 266 nm. While the values for pyrazine dissociation after 248 nm absorption are essentially the same, the values for 266 nm pyrazine dissociation differ by a factor of nearly 2. Obviously, these two plots should yield the same results for the dissociation lifetime since they are simply mathematical rearrangements of the same expression; however, this is only necessarily true if the model used to describe the processes is complete. The model used here only allows for one possible dissociation pathway and in that dissociation pathway the maximum quantum yield has been defined as unity. It is clear from the data that the maximum HCN quantum yield value for the 266 nm data is much less than one by nearly a factor of 2. If this factor of 2 is accounted for properly, the application of Eqs. (16) and (17) to the 266 nm data give the same result. Additionally, because inclusion of all the data produces a plot that is nonlinear, one must arbitrarily choose the linear region of the data, a distinct shortcoming of this model. The deviation from linearity is primarily the result of including only one dissociation pathway accessible to pyrazine, as discussed above. Furthermore, while the intercept for 248 nm excitation is exactly according to model prediction, the intercept for 266 nm excitation using Eq. (16) is significantly greater than 1. While the next model addresses these problems, it should be noted that the long lifetimes estimated using both models are remarkably similar.

A model that is adequate to describe all of the data presented in this paper requires more than one unimolecular dissociation channel. In order to account for a quantum yield that rises above unity, a channel must be added that produces two HCN molecules and C_2H_2 as the fragments. This channel has a lifetime that is much longer than the primary ‘‘late’’ channel producing a single HCN ($k_{d2s} = 1.1 \pm 0.2 \times 10^3 \text{ s}^{-1}$). This rate constant was determined by using a kinetic analysis similar to the one above, simply replacing HCN with C_2H_2 and then using the experimentally measured quantum yields for C_2H_2 rather than HCN to obtain k_{d2s} . One might wonder why the 2-HCN mechanism is not the primary photodissociation mechanism. There are two reasons why this channel is not a principal pathway. While acetylene is detected as mentioned earlier, not enough is observed to support a major role for this step ($\phi_{\text{C}_2\text{H}_2} = 0.03$), and data modeling using a kinetic scheme with this as the only dissociation pathway does not produce convincingly better fits. The second added channel involves ‘‘prompt’’ dissociation to produce HCN, a step that will not be as easily quenched because of the short lifetime of the excited pyrazine. This channel is the result of pyrazine undergoing multiphoton absorption before dissociation as discussed above. The following kinetic scheme is the result of these additions to the model:



The time dependent behavior of the $\text{Pyrazine}^{E'}$, the $\text{Pyrazine}^{2E'}$, and the HCN species can be readily obtained from the differential equations describing the kinetic scheme,

$$\begin{aligned}
[\text{Pyr}^{2E'}] &= [\text{Pyr}^{2E'}]_0 e^{-\gamma t}, \quad \gamma = k_{d1p} + k_{qp}[Q], \\
[\text{Pyr}^{E'}] &= [\text{Pyr}^{E'}]_0 e^{-\gamma' t}, \quad \gamma' = k_{d1s} + k_{d2s} + k_{qs}[Q], \\
[\text{HCN}] &= \frac{k_{d1p}}{\gamma} [\text{Pyr}^{2E'}]_0 (1 - e^{-\gamma t}) \\
&\quad + \frac{k_{d1s} + 2k_{d2s}}{\gamma'} [\text{Pyr}^{E'}]_0 (1 - e^{-\gamma' t}).
\end{aligned} \tag{18}$$

The total number of photons absorbed per unit volume by pyrazine ($N_{h\nu}$) is given by

$$\begin{aligned}
N_{h\nu} &= [\text{Pyr}^{E'}]_0 + 2[\text{Pyr}^{2E'}]_0, \\
N_{h\nu} &= (1 - \alpha)N_{h\nu} + \alpha N_{h\nu},
\end{aligned} \tag{19}$$

where α is a measure of the amount of multiphoton absorption and $\alpha N_{h\nu}/2 = [\text{Pyr}^{2E'}]_0$, while $(1 - \alpha)N_{h\nu} = [\text{Pyr}^{E'}]_0$. Substituting Eqs. (19) into Eqs. (18) gives

$$\begin{aligned}
[\text{Pyr}^{2E'}] &= \frac{\alpha}{2} N_{h\nu} e^{-\gamma t}, \quad \gamma = k_{d1p} + k_{qp}[Q], \\
[\text{Pyr}^{E'}] &= (1 - \alpha) N_{h\nu} e^{-\gamma' t}, \quad \gamma' = k_{d1s} + k_{d2s} + k_{qs}[Q], \\
[\text{HCN}] &= \frac{k_{d1p}}{\gamma} \frac{\alpha}{2} N_{h\nu} (1 - e^{-\gamma t}) \\
&\quad + \frac{k_{d1s} + 2k_{d2s}}{\gamma'} (1 - \alpha) N_{h\nu} (1 - e^{-\gamma' t}).
\end{aligned} \tag{20}$$

At long times this can be rearranged to give

$$\begin{aligned}
\phi &= \frac{[\text{HCN}]}{N_{h\nu}} = \frac{k_{d1p}}{\gamma} f_p + \frac{k_{d1s} + 2k_{d2s}}{\gamma'} f_s, \\
f_p &= \frac{[\text{Pyr}^{2E'}]_0}{N_{h\nu}} = \frac{\alpha}{2}; \quad f_s = \frac{[\text{Pyr}^{E'}]_0}{N_{h\nu}} = (1 - \alpha).
\end{aligned} \tag{21}$$

In this expression for ϕ , the first term, $k_{d1p}f_p/\gamma$, is associated with the ‘‘prompt’’ ‘‘unquenched’’ channel. Regardless

of the pressure used in the present experiments, this term is not eliminated and is, therefore, essentially constant with respect to the collision rate ($\gamma \sim k_{d1p} \gg k_{qp}[Q]$). This term can be identified as the quantum yield for the unquenched channel, $\phi_u \approx f_p$. Such a definition is consistent with the idea of an ‘‘unquenched channel’’ since all the pyrazine excited initially by the UV light to $\text{Pyr}^{2E'}$ becomes HCN, and the production of $\text{Pyr}^{2E'}$ requires the absorption of two photons; thus,

$$\phi_u = \frac{[\text{HCN}]_{\text{prompt}}}{N_{h\nu}} = \frac{[\text{Pyr}^{2E'}]_0}{N_{h\nu}} = f_p.$$

As has been discussed above, this ‘‘prompt’’ channel is pump laser intensity dependent and its quantum yield, ϕ_u , can be estimated for 248 nm dissociation using Eq. (12) to give a value of $\phi_u = 0.02 \pm 0.01$ (laser fluence of 9.5 mJ/cm²).

Equation (21) can then be rearranged expressing ϕ as a function of t_{coll} ,

$$\phi = \left(\frac{1}{\phi_m} + \frac{t_d}{t_{\text{coll}}} \right)^{-1} + \phi_u, \tag{22}$$

where $t_d = 1/(k_{d1s} + 2k_{d2s})f_s$ is the effective lifetime of excited pyrazine, $\phi_m = (k_{d1s} + 2k_{d2s})f_s/(k_{d1s} + k_{d2s})$ is the maximum quantum yield from the ‘‘late’’ channel in the absence of quenching, and $t_{\text{coll}} = 1/k_{qs}[Q]$ is the mean hard sphere collision time. To allow for easier comparison with the earlier model [described by Eq. (16)], we rearrange this to

$$\frac{1}{\phi - \phi_u} = \frac{t_d}{t_{\text{coll}}} + \frac{1}{\phi_m}, \tag{23}$$

which simplifies to Eq. (16) if there is neither a ‘‘prompt’’ channel ($\phi_u = 0$) or a 2 HCN channel ($\phi_m = 1, k_{d2s} = 0$). In this kinetic analysis, the dissociation lifetime, t_d , reflects the overall lifetime for the ‘‘late’’ channel. Disregarding k_{d1p} for the moment, ϕ_m can range from $f_s(k_{d1s} \gg k_{d2s})$ to $2f_s(k_{d1s} \ll k_{d2s})$ depending on the competition between the two ‘‘late’’ channels identified above.

Equation (22) forms the basis for a three-parameter, non-linear least squares fit that determines t_d , ϕ_m , and ϕ_u for each data set in the self-quenching, and SF₆ and CO₂

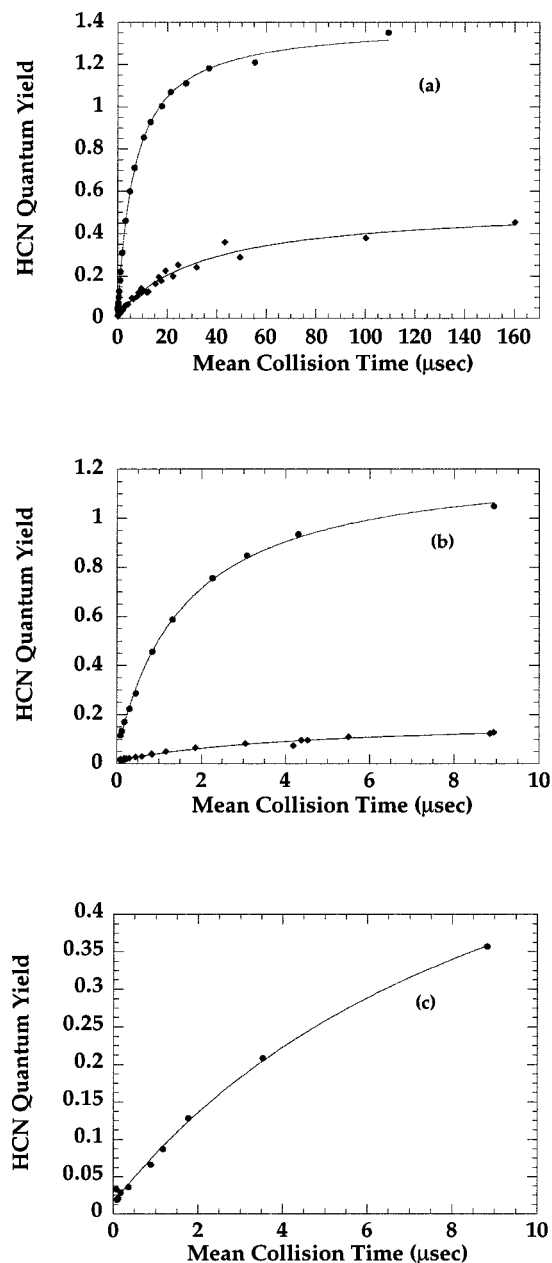


FIG. 10. Quantum yield displayed as a function of the mean collision time for (a) self-quenching studies, (b) CO_2 -quenching studies, and (c) SF_6 -quenching. Circles are for 248 nm excitation while diamonds are for 266 nm excitation. The solid lines are the result of a three-parameter, nonlinear least-squares fit to the data using Eq. (22). The results of this nonlinear fit are summarized in Table III. These data provide a value of $1.69 \times 10^5 \text{ s}^{-1}$ and $1.33 \times 10^4 \text{ s}^{-1}$ for the first order photodissociation rate constant for self-quenching 248 and 266 nm studies, respectively; $8.33 \times 10^5 \text{ s}^{-1}$ and $3.44 \times 10^4 \text{ s}^{-1}$ for CO_2 quenching 248 and 266 nm studies, respectively; and $7.27 \times 10^5 \text{ s}^{-1}$ for SF_6 quenching 248 nm studies. Quantum yield measurements obtained for 248 nm and 266 nm excitation were conducted at an UV laser fluence of 9.5 mJ/cm^2 and 5.0 mJ/cm^2 , respectively.

quenching groups of data. Figure 10 displays the resulting fits, and Table III summarizes the parameters. The 248 nm excited pyrazine lifetime of $6.2 \pm 0.4 \mu\text{s}$ derived from this data is in good agreement with the results of previous studies ($6.6 \mu\text{s}$),⁴³ in spite of the fact that more channels have been considered in this analysis. This is one indication that these additional channels are responsible for only a small fraction

of the overall HCN yield. Note also that the lifetime for pyrazine excited to 37910 cm^{-1} is even longer than this ($\sim 70 \mu\text{s}$), highlighting the fact that these molecules with “chemically significant” amounts of internal energy can live for a very long time before fragmenting, especially near the reaction threshold energy.

The pyrazine dissociation rate under self-quenching conditions is smaller ($1.69 \times 10^5 \text{ s}^{-1}$) than for either SF_6 quenching ($7.27 \times 10^5 \text{ s}^{-1}$) or CO_2 quenching ($8.33 \times 10^5 \text{ s}^{-1}$) following 248 nm excitation. This is the same trend observed for self-quenching and CO_2 quenching after 266 nm excitation, $1.33 \times 10^4 \text{ s}^{-1}$ (self) and $3.44 \times 10^4 \text{ s}^{-1}$ (CO_2), respectively. This is again consistent with the earlier qualitative observation that both SF_6 and CO_2 are less effective than unexcited pyrazine at quenching excited pyrazine, and is merely a consequence of applying the strong collision model indiscriminately to all quenchers. The strong collision model is certainly most appropriate for a bath gas which carries away a large amount of energy upon each collision, and hence the rate constant extracted from the pyrazine self-quenching data is the most reliable value in the context of the strong collision model. Because higher pressures of either SF_6 or CO_2 are required to be as effective as pyrazine at quenching fragmentation, the dissociation rates for pyrazine derived from the SF_6 and CO_2 data are larger, a result of the strong collision model. Because unexcited pyrazine is the most efficient strong collision partner of the three, the dissociation rate constant from self-quenching data is then an *upper limit* for the dissociation process; in other words, the “true” dissociation rate for pyrazine must be even smaller than measured here! Thus, the lifetime of the excited pyrazine is even longer than 6.2 and $66 \mu\text{s}$ for 248 nm and 266 nm excitation, respectively. Note also that the *differences* in the lifetime between self quenching and CO_2 quenching are smaller at 37910 cm^{-1} than at 40640 cm^{-1} indicating (as expected) that pyrazine is much closer to its critical energy, E_0 , for fragmentation to form HCN at 37910 cm^{-1} than at 40640 cm^{-1} .

This second model provides a reasonable basis for analyzing results where ϕ_m is unity or even greater than unity; however, for the 266 nm self-quenching data ϕ_m falls well below 1 ($\phi_m = 0.52$). For these results to make sense, there must be some “dark” channel that does not produce HCN available to pyrazine excited by 266 nm radiation. It is possible that pyrazine with $E_{\text{int}} = 37910 \text{ cm}^{-1}$ is so close to E_0 , the energy threshold for dissociation, that the excited pyrazine is distributed on both sides of E_0 reflecting the thermal energy spread of initially unexcited pyrazine. 266 nm excitation also provides the longest dissociation lifetimes, $\approx 70 \mu\text{s}$; this time scale is in the range of IR fluorescence lifetimes for highly vibrationally excited states. Photodissociation at even the lowest pressures may, thus, be in competition with radiative quenching processes.^{1–3,39,58} This effect has been ignored in the present analysis, as have wall collisions. Both of these effects will lead to an apparent $\phi_m < 1$.

V. CONCLUSIONS

This work combines both experimental and theoretical studies to provide greater insight into the dissociation of

TABLE III. HCN quantum yields, photodissociation lifetimes, and photodissociation rate constants for the 248 nm and 266 nm photofragmentation of pyrazine as derived from fits to the data shown in Fig. 10 using Eq. (22).^a

Quencher	Excitation wavelength (nm)	ϕ_m^b	ϕ_u^c	t_d^d	k_{d1s}^e
Self	248	1.3 ± 0.2	0.03 ± 0.01	6.2 ± 0.4	1.69×10^5
SF ₆	248	0.7 ± 0.2	0.02 ± 0.01	1.4 ± 0.1	7.27×10^5
CO ₂	248	1.2 ± 0.2	0.04 ± 0.01	1.3 ± 0.1	8.33×10^5
Self	266	0.5 ± 0.3	0.012 ± 0.004	66 ± 4	1.33×10^4
CO ₂	266	0.17 ± 0.03	0.013 ± 0.002	28 ± 3	3.44×10^4

^aAll data was collected at $I_{\text{laser}} = 9.5 \pm 1 \text{ mJ/cm}^2$.

^bThe maximum value for the quantum yield. $\phi_m = (k_{d1s} + 2k_{d2s})f_s / (k_{d1s} + k_{d2s})$, see text following Eqs. (22) and (23) for definitions of symbols.

^cThe quantum yield for the “prompt” “unquenched” channel. $\phi_u = f_p$, see text following Eq. (21) for definitions of symbols.

^dThe photodissociation lifetime (i.e., the lifetime of vibrationally excited pyrazine) given in microseconds. $t_d = 1 / (k_{d1s} + 2k_{d2s})f_s$, see text following Eqs. (22) and (23) for definitions of symbols.

^eRate constant for the dissociation of pyrazine given in units of sec^{-1} and determined using the expression for t_d above, where $k_{d2s} = 1.1 \times 10^3$ was obtained from probing the C₂H₂ yield as described in the text.

highly vibrationally excited azabenzenes, in particular pyrazine, following absorption of UV laser radiation. Experimentally, the HCN quantum yield has been measured using high resolution IR diode probing of the HCN photoproduct as a function of quencher gas pressure and UV laser intensity. At low pressures, the effect of changing UV pump laser intensity on quantum yields is small, while at high pressures the HCN quantum yield shows a strong positive correlation with changes in pump laser fluence. This quenching study provides a highly sensitive means of observing photodissociation via a multiphoton channel. Additionally, the amount of HCN produced via an “unquenched” multiphoton process can be determined if the intensity of the pump laser is known. The extreme sensitivity of this quenching approach to the study of multiphoton absorption is a direct result of the fact that at high quencher gas pressures all one-photon photochemistry can be essentially eliminated.

Additionally, the information theoretic prior functions for energy disposal in the photodissociation of pyrazine to form HCN and C₃H₃N have been developed. These surprisal distributions correspond nicely with previous molecular beam studies of this dissociation;⁴¹ further, they correlate most of the high velocity HCN with two- and three-photon dissociation processes. Essentially, all fast moving HCN is predicted to come from pyrazine that has undergone multiphoton absorption, while all HCN produced from pyrazine that has absorbed only one-photon is predicted to have a relatively small amount of translational energy ($<6 \text{ kcal/mol}$, $\langle E \rangle = 2.65 \text{ kcal/mol}$), about four times the average translational energy at room temperature (RT = 0.596 kcal/mol , $T = 300 \text{ K}$).

Finally, IR diode probing of the HCN photoproduct in the dissociation of pyrazine has been used to determine the HCN quantum yield at both 248 nm and 266 nm. A hard collision kinetic model of the data has been employed to determine the time scale of the dissociation process ($6.2 \pm 0.4 \mu\text{s}$ and $66 \pm 4 \mu\text{s}$ following 248 nm and 266 nm excitation, respectively).

The effect of HCN, produced by both single and multiphoton absorption, on the energy transfer dynamics in

pyrazine/CO₂ mixtures excited by 248 and 266 nm laser radiation, is discussed in the following paper.

ACKNOWLEDGMENTS

The authors thank Dr. Jack Preses, Dr. Greg Hall, Dr. Trevor Sears, and Dr. Ralph Weston, and Professors Amy Mullin and Simon North for many stimulating and provocative discussions. Work described here and performed at Columbia University was supported by the Department of Energy under Grant No. DE-FG02-88ER13937. Equipment support was provided by the National Science Foundation under Grant No. CHE-97-27205 and the Joint Service Electronic Program (U.S. Army, U.S. Navy, and U.S. Air Force) under Contract No. DAAG55-97-I-0166. Work performed at Brookhaven National Laboratory was carried out under Contract No. DE-AC02-76CH00016 with the U.S. Department of Energy and supported by its Division of Chemical Sciences, Office of Basic Energy Sciences. E.T.S. acknowledges support from the Edwin A. Link Energy Foundation, M.A.M. acknowledges sabbatical support from Calvin College and the Calvin College-Howard Hughes Medical Institute Grant, and S.M.R. acknowledges support from the Columbia College Rabi Scholars Program and the V. Kann Rasmussen Foundation.

¹D. B. McDonald and S. A. Rice, *J. Chem. Phys.* **74**, 4907 (1981).

²T. J. Bevilacqua, B. K. Andrews, J. E. Stout, and R. B. Weisman, *J. Chem. Phys.* **92**, 4627 (1990).

³T. J. Bevilacqua and R. B. Weisman, *J. Chem. Phys.* **98**, 6316 (1993).

⁴D. R. McDowell, F. Wu, and R. B. Weisman, *J. Phys. Chem. A* **101**, 5218 (1997).

⁵R. B. Weisman, in *Advances in Chemical Kinetics and Dynamics: Vibrational Energy Transfer Involving Large and Small Molecules*, edited by J. R. Barker (JAI, Greenwich, CT, 1995), Vol. 2B, p. 333.

⁶M. Damm, H. Hippler, H. A. Olschewski, J. Troe, and J. Willner, *Z. Phys. Chem., Neue Folge* **166**, 129 (1990).

⁷M. Damm, F. Deckert, H. Hippler, and J. Troe, *J. Phys. Chem.* **95**, 2005 (1991).

⁸H. Hippler and J. Troe, in *Bimolecular Collisions*, edited by M. N. R. Ashfold and J. E. Baggott (Royal Society of Chemistry, London, 1989).

⁹L. A. Miller and J. R. Barker, *J. Chem. Phys.* **105**, 1383 (1996).

- ¹⁰L. A. Miller, C. D. Cooks, and J. R. Barker, *J. Chem. Phys.* **105**, 3012 (1996).
- ¹¹B. M. Toselli and J. R. Barker, *J. Chem. Phys.* **95**, 8108 (1991).
- ¹²B. M. Toselli, J. D. Brenner, M. L. Yerram, W. E. Chin, K. D. King, and J. R. Barker, *J. Chem. Phys.* **95**, 176 (1991).
- ¹³B. M. Toselli and J. R. Barker, *J. Chem. Phys.* **97**, 1809 (1992).
- ¹⁴M. L. Yerram, J. D. Brenner, K. D. King, and J. R. Barker, *J. Phys. Chem.* **94**, 6341 (1990).
- ¹⁵J. D. Brenner, J. P. Erinjeri, and J. R. Barker, *Chem. Phys.* **175**, 99 (1993).
- ¹⁶T. G. Dietz, M. A. Duncan, A. C. Pulu, and R. E. Smalley, *J. Phys. Chem.* **86**, 4026 (1982).
- ¹⁷J. Knee and P. Johnson, *J. Phys. Chem.* **89**, 948 (1985).
- ¹⁸P. A. M. Ujit de Haag and W. L. Meerts, *Chem. Phys.* **135**, 139 (1989).
- ¹⁹O. Sneh, D. Dünn-Kittenplon, and O. Cheshnovsky, *J. Chem. Phys.* **91**, 7331 (1989).
- ²⁰R. E. Weston, Jr. and G. W. Flynn, *Annu. Rev. Phys. Chem.* **43**, 559 (1992).
- ²¹G. W. Flynn and R. E. Weston, Jr., in *Advances in Chemical Kinetics and Dynamics: Vibrational Energy Transfer Involving Large and Small Molecules*, edited by J. R. Barker (JAI, Greenwich, CT, 1995), Vol. 2B, p. 359.
- ²²G. W. Flynn, C. S. Parmenter, and A. M. Wodtke, *J. Phys. Chem.* **100**, 12817 (1996).
- ²³G. W. Flynn, C. A. Michaels, H. C. Tapalian, Z. Lin, E. T. Sevy, and M. A. Muyskens, in *Highly Excited Molecules: Relaxation, Reaction, and Structure*, edited by A. S. Mullin and G. C. Schatz (American Chemical Society, Washington, D.C., 1997), p. 134.
- ²⁴C. A. Michaels, A. S. Mullin, and G. W. Flynn, *J. Chem. Phys.* **102**, 6682 (1995).
- ²⁵C. A. Michaels, A. S. Mullin, J. Park, J. Z. Chou, and G. W. Flynn, *J. Chem. Phys.* **108**, 2744 (1998).
- ²⁶A. S. Mullin, J. Park, J. Z. Chou, G. W. Flynn, and R. E. Weston, Jr., *Chem. Phys.* **175**, 53 (1993).
- ²⁷A. S. Mullin, C. A. Michaels, and G. W. Flynn, *J. Chem. Phys.* **102**, 6032 (1995).
- ²⁸C. A. Michaels and G. W. Flynn, *J. Chem. Phys.* **106**, 3558 (1997).
- ²⁹R. G. Gilbert and S. C. Smith, *Theory of Unimolecular and Recombination Reactions* (Blackwell Scientific, Oxford, 1990).
- ³⁰K. E. Wilzbach, A. L. Harkness, and L. Kaplan, *J. Am. Chem. Soc.* **90**, 116 (1968).
- ³¹K. E. Wilzbach, A. L. Harkness, and L. Kaplan, *J. Am. Chem. Soc.* **90**, 3291 (1968).
- ³²Y. T. Lee, 185th American Chemical Society National Meeting, Toronto, Canada, 1988 (unpublished).
- ³³J. D. Chesko, D. Stranges, A. G. Suits, and Y. T. Lee, *J. Chem. Phys.* **103**, 6290 (1995).
- ³⁴N. Nakashima and K. Yoshihara, *Bull. Chem. Soc. Jpn.* **55**, 2783 (1982).
- ³⁵N. Nakashima and K. Yoshihara, *J. Chem. Phys.* **77**, 6040 (1982).
- ³⁶J. M. Preses, G. E. Hall, J. T. Muckerman, T. J. Sears, and R. E. Weston, Jr. (in preparation).
- ³⁷J. H. Kiefer, Q. Zhang, R. D. Kern, J. Yao, and B. Jursic, *J. Phys. Chem. A* **101**, 7061 (1997).
- ³⁸R. E. Weston, Jr. (personal communication).
- ³⁹I. Yamazaki, T. Murao, T. Yamanaka, and K. Yoshisara, *Faraday Discuss. Chem. Soc.* **75**, 395 (1983).
- ⁴⁰A. Doughty, J. C. Mackie, and J. M. Palmer, presented at the Twenty-Fifth Symposium (International) on Combustion/The Combustion Institute, 1994 (unpublished).
- ⁴¹J. D. M. Chesko, Ph.D., University of California, 1995.
- ⁴²J. D. Chesko and Y. T. Lee, in *Highly Excited Molecules: Relaxation, Reaction, and Structure*, edited by A. S. Mullin and G. C. Schatz (American Chemical Society, Washington, D.C., 1997), pp. 107–120.
- ⁴³C. A. Michaels, H. C. Tapalian, Z. Lin, E. T. Sevy, and G. W. Flynn, *Faraday Discuss.* **102**, 405 (1995).
- ⁴⁴E. T. Sevy, C. A. Michaels, H. C. Tapalian, and G. W. Flynn, *J. Chem. Phys.* **112**, 5844 (2000), following paper.
- ⁴⁵G. W. Flynn and R. E. Weston, Jr., *J. Phys. Chem.* **97**, 8116 (1993).
- ⁴⁶G. S. Ondrey and R. Bersohn, *J. Chem. Phys.* **81**, 4517 (1984).
- ⁴⁷S. R. Goates, J. O. Chu, and G. W. Flynn, *J. Chem. Phys.* **81**, 4521 (1984).
- ⁴⁸H. Okabe, *Photochemistry of Small Molecules* (Wiley, New York, 1978).
- ⁴⁹L. A. Pugh and K. N. Rao, in *Molecular Spectroscopy: Modern Research*, edited by K. N. Rao (Academic, New York, 1976), Vol. II.
- ⁵⁰L. S. Rothman, R. R. Gamache, A. Barbe, A. Goldman, J. R. Gillis, L. R. Brown, R. A. Toth, J. M. Flaud, and C. Camy-Peyret, *Appl. Opt.* **22**, 2247 (1983).
- ⁵¹J. R. Barker and B. M. Toselli, *Int. Rev. Phys. Chem.* **12**, 305 (1993).
- ⁵²M. A. Muyskens and E. T. Sevy, *J. Chem. Educ.* **74**, 1138 (1997).
- ⁵³A. Bolovinos, P. Tsekeris, J. Philis, E. Pantos, and G. Andritsopoulos, *J. Mol. Spectrosc.* **103**, 240 (1984).
- ⁵⁴J. T. Muckerman, *J. Phys. Chem.* **93**, 179 (1989).
- ⁵⁵J. D. Simmons and K. K. Innes, *J. Mol. Spectrosc.* **14**, 190 (1964).
- ⁵⁶*CRC Handbook of Chemistry and Physics* (Chemical Rubber, Cleveland, 1973).
- ⁵⁷M. N. Glukhovtsev (personal communication).
- ⁵⁸J. R. Barker, J. D. Brenner, and B. M. Toselli, in *Advances in Chemical Kinetics and Dynamics: Vibrational Energy Transfer Involving Large and Small Molecules*, edited by J. R. Barker (JAI, Greenwich, 1995), Vol. 2B, p. 393.